Experiments on magnetic interference for a portable airborne magnetometry system using a hybrid unmanned aerial vehicle (UAV)

Jirigalatu Jirigalatu, Vamsi Krishna, Eduardo Lima Simões da Silva, and Arne Døssing

CMAGTRES, Technical University of Denmark
Centrifugevej Bygning 356
2800 Kgs. Lyngby, Denmark

Correspondence: Arne Døssing (ards@space.dtu.dk)

Abstract. Airborne magnetic surveys are an important and efficient tool for mapping the subsurface, providing insights e.g. into mineral deposits. Compared to traditional ground methods, airborne magnetic surveys offer great advantages with improved access and rapid sampling. But the cost and hassle of transporting and operating a conventional manned airborne magnetic survey system are strong impediments for its wider use. In addition, the conventional airborne systems are challenged by the need for low-altitude (≤ 80 m) surveying to detect small-scale subsurface features evident in ground surveys. Portable and compact airborne magnetic survey systems using unmanned aerial vehicles (UAVs) can not only bridge the gap between conventional airborne magnetic surveys and ground magnetic surveys but also complement magnetic surveys to fit broader geophysical applications. Therefore, developing high-quality, stable, and portable UAV-borne survey systems is of high interest to the geophysical exploration community. However, developing such a system is challenging owing to strong magnetic interference introduced by onboard electric engines and other onboard electronic devices. As a result, tests concerning the static and dynamic magnetic interference of a UAV are critical to assess the severity of the interference and can help to improve the design of the system at the early stage of development. A static experiment and two dynamic experiments were conducted to understand the characterization of the magnetic interference of our hybrid vertical take-off and landing (VTOL) UAV. The results of the static experiment show that the wing area is highly magnetic due to the proximity to servomotors and motors, but the area along the longitudinal axis of the UAV is relatively magnetically quiet. To reduce the magnetic signature, the highly-magnetic servomotors on the wings were replaced with less magnetic servomotors of a brush-less type. Assisted by aerodynamic simulations, we further designed a front-mounting solution for two compact magnetometers. Two dynamic experiments were conducted with this setup to understand the dynamic interference of the UAV in operation. The results of the dynamic experiments reveal that the strongest source of in-flight magnetic interference is mainly due to the cables connecting the battery to the flight controller and that this effect is most influential during pitch maneuvers of the aircraft.

1

Geoscientific
Instrumentation
Methods and
Data Systems
Discussions

1 Introduction

Magnetic surveying has been extensively used in the search for mineral deposits, oil and gas reservoirs, geothermal resources, as well as for a variety of other purposes such as natural hazards assessment, basement structural studies, mapping subsurface archaeology and unexploded ordnance (UXO) (Nabighian et al., 2005; Eppelbaum, 2011; Fairhead, 2012; Hinze et al., 2013;

25 Eppelbaum, 2015; Kruse, 2013; Haldar, 2018; Turner et al., 2015; Zhou, 2018). In general, magnetic measurements can provide information on and insight into the physical, chemical, and even biological processes that have affected the iron phases within.

Airborne magnetometry (aeromagnetometry) is an inexpensive, efficient, and effective regional reconnaissance tool (Reeves, 2005; Eppelbaum, 2015; Haldar, 2018). The method offers improved accessibility to areas restricted to terrestrial surveys such as remote areas, offshore areas, and thickly-vegetated regions as well as rapid sampling of the local geomagnetic field compared

30 to its ground or space counterpart (Council, 1995; Haldar, 2018).

Traditionally, aeromagnetic surveys are often conducted using fixed-winged aircraft with sensors mounted on both the wings (horizontal sensor configuration) or a tail-boom behind the aircraft. Thanks to decades of development and noise reduction techniques coupled with new advances in sensor technologies, such modern aeromagnetic surveys can achieve a sensitivity of 0.1 nanoTesla (nT) (Eppelbaum, 2015; Aminzadeh and Dasgupta, 2013; Turner et al., 2015). However, geophysicists have

35 realized that aeromagnetometry using light-weight and compact platforms such as unmanned aerial vehicles (UAV) can even further reduce the surveying cost and make it more convenient in terms of logistics (Eppelbaum and Mishne, 2011; Tuck et al., 2018; Mu et al., 2020). Besides, traditional manned aeromagnetic surveys normally operate at 80 meters or above for the safety of personnel and because of flight regulations, whereas UAV-borne magnetometry systems are capable of flying at a lower altitude, thereby improving detectability (Reid, 1980; Reeves et al., 1997; Eppelbaum and Mishne, 2011; Zhou, 2018).

40 In the recent decade, the feasibility and effectiveness of light-weight UAV-borne magnetometry systems have been demonstrated again and again by various geophysical applications, from identifying various rock types and structures in the subsurface and delineating ore deposits to locating man-made ferrous objects, such as UXO (Perry et al., 2002; Cunningham, 2016; Malehmir et al., 2017; Parvar et al., 2017; Kolster and Døssing, 2020). However, developing a low-noise and efficient UAV-borne magnetometry system is challenging given the compact space of a UAV platform, i.e., magnetometers readily fall in the

45 vicinity of sources of magnetic interference from the platform, such as motors, electric powered devices, and even current-carrying wires (Forrester, 2011; Sterligov and Cherkasov, 2016; Tuck et al., 2018). As a result, UAV-borne magnetometry systems are operated often by suspending a so-called magnetometer bird (housing magnetometers, global positioning system (GPS) antenna and data logger) a few meters below the airframe to minimize the interference from the platform (Malehmir et al., 2017; Parvar et al., 2017; Parshin et al., 2018; Sterligov et al., 2018; Nikulin and de Smet, 2019). This configuration

50 is hardly prone to the onboard magnetic interference from the platform but comes with a cost of efficiency and positioning accuracy (Tuck et al., 2018). Alternatively, magnetometers may be mounted directly on a boom attached to the UAV airframe (Samson et al., 2010) or on the wing-tips of the platform (Wood et al., 2016).

To facilitate high-quality and efficient UAV-borne magnetometry, we intend to develop a lightweight (less than 10 kg), efficient (more than 70 km per charge), and flexible (vertical take-off and landing) UAV-borne magnetometry system, capable

55 of conducting magnetic surveys in various terrains. To meet the requirements, we chose a hybrid lightweight fixed-wing UAV

platform capable of taking off and landing vertically. But where and how to put the magnetometers on the UAV are the first

challenge we have to face. Hence, a good understanding of the magnetic interference of the platform is necessary at the early

stage of the development. For example, Forrester (2011) and Sterligov and Cherkasov (2016) successfully mapped magnetic

signatures of the UAVs and also managed to locate sources of interference. However, they neglected to address the complex

60 interplay between active and passive components (Tuck et al., 2018). Therefore, Tuck et al. (2018) proposed a systematic

method to investigate magnetic interference of UAVs and demonstrated their method on a 25 kg fixed-wing UAV. However,

the method is still not sufficient to cover the actual interplay between static interference and dynamic interference in operation.

In this paper, we will present a static and two dynamic experiments to investigate both the static and dynamic magnetic

interference from the platform in operation.

2 Platform - A hybrid VTOL UAV

The UAV for our airborne magnetometry system is a beta prototype version of a hybrid vertical take-off and landing (VTOL)

UAV from Kapetair. As the name of the UAV indicates, the UAV is capable of taking off and landing vertically without a

runway, so it can be deployed in various terrains. Since the UAV is a hybrid, it is capable of flying both in multi-rotor mode

and fixed-wing mode. The UAV has three position-adjustable motors. The two front motors are mainly used for taking off and

70 landing. The third (tail) motor is used for take-off and landing as well as to provide thrust during the fixed-wing cruise mode,

i.e., the front motor stays inactive during the cruise mode and only the rear engine remains active. The main fuselage of the

UAV houses various hardware components, including a flight controller (FC), several electronic speed controllers (ESC), an

inertial measurement unit (IMU), a global positioning system (GPS) module, a radio-frequency (RF) module, a data-logger for

magnetometry, and a few wires or cables connecting those components. A 22000 mAh Li-Po battery is also placed inside in

75 the fuselage. The technical specifications of the platform are listed in Table 1.

2.1 Source of magnetic interference

For a lightweight UAV platform such as the Kapetair VTOL UAV, brushless direct current (BLDC) motors are often used due to

their better speed control, higher efficiency, and compact design A. D. P. Juliani et al. (2008). However, BLDC motors comprise

permanent magnets and solenoids. Hence, the electric engines and the servomotors generate a strong magnetic signature even

80 when they are off and leakage of a strong magnetic field when they are on. Besides, the BLDC motors are driven to revolve

at the desired speed by sending properly tuned pulses of current to the solenoids, which means constant electrical switching,

probably causing discontinuous in-flight magnetic measurements. Tuck et al. (2018) observed magnetic interference due to

the current-carrying wires connecting the ESC to the batteries. According to Ampere's law, the magnetic field is proportional

to the electric current, therefore, the magnetic interference varies linearly with the current in the wires. Moreover, the airframe of the

85 UAV is composed of carbon fiber, which is non-magnetic but conductive, akin to graphite (Chung, 2010). As a result, eddy

currents (Richard L., 1974) may play a role in magnetic interference during a flight. Finally, the onboard avionics system

3

Table 1. Specifications of Kapetair VTOL UAV

Component of the UAV	
Dimensions	wingspan×length 3300 ×1670 mm
Batteries	1 6S Li-Po 22.2V 488.4 Wh 22000 mAh
Servomotors on the wings	4 HBL 6625MINI Metal Alloy Gear
Propulsion system	3 T-Motor MN5212 KV420 BLDC motor
Flight controller	Pixhawk 2
Payload weight	1000 g
Cruise speed	65 km/h
Aircraft gross weight	6.5 kg
Stall speed (airplane mode)	20 km/h

I also see Servomotor & engine used... (handwritten annotation)

which comprises several electronic components (such as the FC module, the IMU module, the GPS module, etc.) may generate complex electromagnetic interference. A rule of thumb is therefore always to place magnetometers as far away from the magnetic UAV components as possible.

90 3 UAV magnetic signature mapping - static experiment

An airborne magnetometry system using a compact UAV platform is affected by the UAV's magnetic signature (Tuck et al., 2018). Mapping the magnetic signature of a UAV is useful to identify highs and lows of the UAV's own magnetic field and helps us to avoid magnetic highs when developing our magnetometry system and pinpoint the favorable regions less susceptible to the UAV's magnetic interference. However, the magnetic signature varies from platform to platform, and it is therefore imperative

95 to map a platform's specific magnetic signature to identify sources of interference and pinpoint optimal regions on the aircraft for mounting magnetometers.

3.1 Method

The magnetic signature mapping of the Kapetair UAV was carried out at the Brorfelde geomagnetic observatory in Denmark. A customized 2300×958×700 mm wooden frame was built for the experiment (Fig 1). Since the magnetic signature of a UAV

100 can change significantly over a few centimeters, it is beneficial to have the magnetic signature on a fine grid such as a 10×10 cm cell (Sterligov and Cherkasov, 2016). However, such an approach is time-consuming if carried out manually. We adopted a slowly revolving DC motor to pull a slider holding a high-precision potassium scalar magnetometer (GSMP-35U from GEM Systems). The sampling rate of the magnetometer was set to 10 Hz and the speed of the slider was 2 cm/s on average. The motor, a laptop for data logging, and two power supplies were placed in another room away from the measurement. Due to
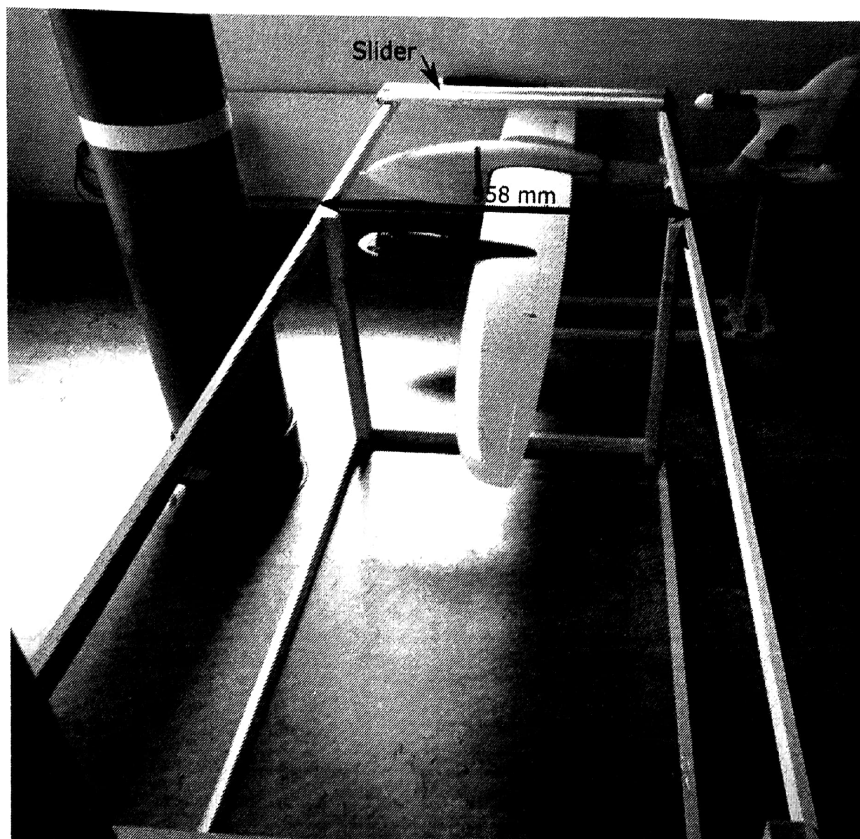
Figure 1. Demonstration of the magnetic signature measurement of the port wing. The length and width of the slider are 1000 and 150 mm, respectively.

105   the limited space in the observatory, only one wing and the mainframe were measured at once (Fig 1). The UAV remained turned-off during the magnetic signature measurement.
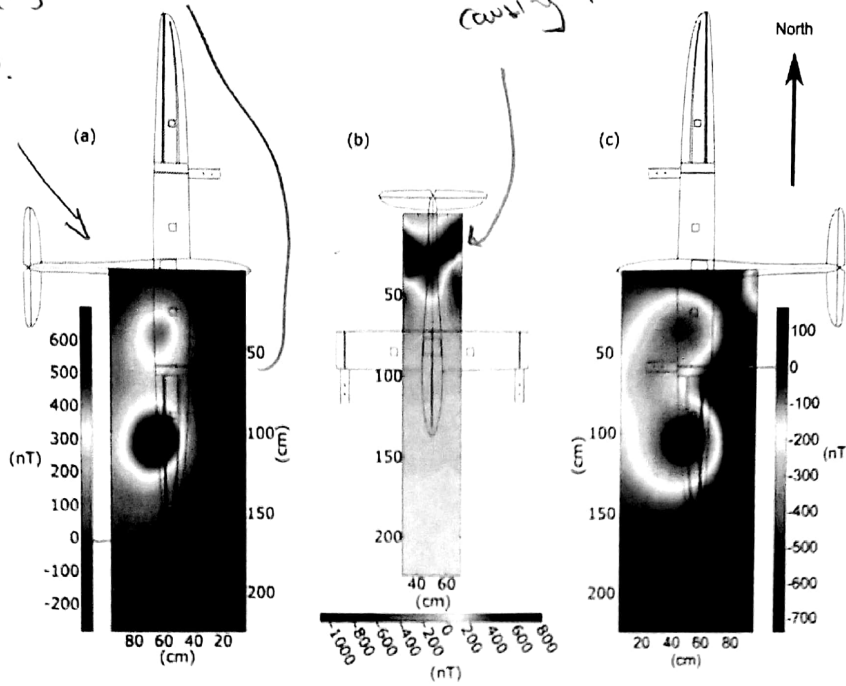
3.2 Magnetic signature

With the help of the semi-automatic magnetic measurement, we managed to collect more than 70,000 magnetic observations of the UAV magnetic signature, including the starboard wing, the port wing, and the area along the longitudinal axis of the

110   UAV (Fig 2). As seen in 2 the magnetic signature of the wing area has a high amplitude (up to + 600 nT) and peaks over the servomotors and the motors. Interestingly, the servomotors signal is asymmetric, being significantly higher over the outer starboard wing as compared to the outer port wing. As expected the servomotors signal rapidly decreases with distance, also towards the main fuselage of the platform. It is axiomatic that the servomotors make a major contribution to the magnetic signature. However, for a high-resolution aeromagnetic system, the standard of commercial aeromagnetic practice only allows a

115   noise envelope of 0.1 nT after compensation, assuming that post compensation can remove 95% percent or more of interference from aeromagnetic data Reeves (2005); Tuck et al. (2018). This, on the other hand, requires the magnetometers to be mounted

5

Figure 2. The diurnal-corrected and background-subtracted magnetic signature: (a) the starboard wing, (b) the area along the longitudinal axis of the UAV, and (c) the port wing.

in places with the least magnetic signature. Due to the high magnetic signature of the servomotors, we decided to replace the originally highly magnetic servomotors with more expensive BLDC servomotors with a smaller magnetic signature (see 3).
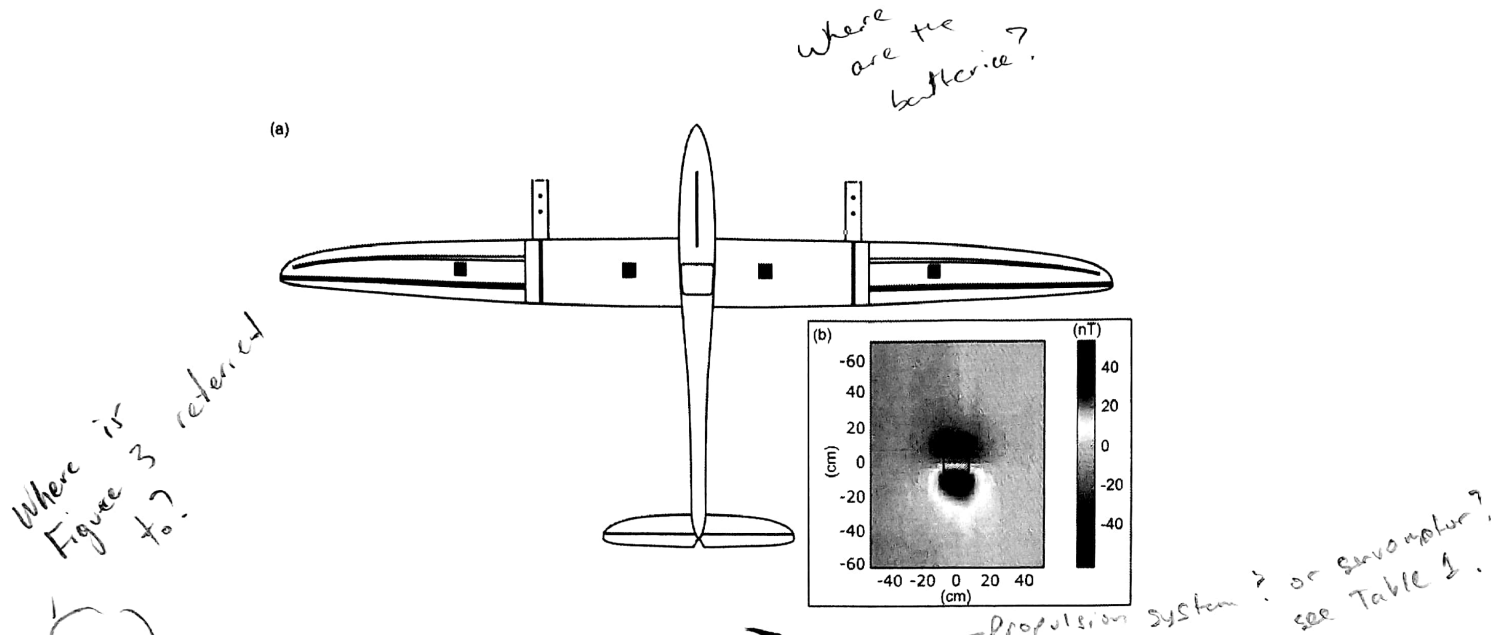
According to the map of the magnetic signature (Fig 2), the wing-tips and the nose-tip are magnetically low-amplitude zones. Mounting two magnetic sensors at the tip of the wings enable us to measure the horizontal gradient, which is useful for both data processing and interpretation purposes. However, the wings are deliberately flexible to adapt to dynamic airflow in flight, i.e. the high-frequency vertical displacement due to the flexibility (readily up to 120 mm during flight (Tuck et al., 2018)) may introduce unpredictable noise Kaneko et al. (2011). Moreover, aerodynamically, the wingtips are sensitive to the disturbance caused by geometric changes, i.e., mounting magnetometers onto the wings' exterior may lead to wing stall and even a crash.

4 A front-boom setup

Mounting magnetometers on the nose-tip does not provide a typical horizontal gradient but, on the other hand, provides an aerodynamically safe and stable solution. To avoid the risk of aerodynamic instability, we designed a magnetometry system mounting on the nose of the UAV using protruding carbon rods (see Fig 4). This configuration will theoretically not cause any aerodynamic instability because the geometric modification to the nose area should cause only small aerodynamic forces. We carried out a computational fluid dynamics (CFD) simulation on the fuselage to investigate the aerodynamic stability of the

(handwritten annotations: where the ...
are the ...
better?)

(a)

(handwritten: Where is reference)
(handwritten: Where is Figure 3 to?)
(handwritten: Propulsion System? or Servomotor, see Table 1.)

(b) (nT)

Figure 3. Locations of the servomotors and the magnetic signature of the new BLDC servomotor. (a) the locations of the replaced servomotors, which are indicated by green squares, (b) the magnetic signature of the new low-magnetic servomotor, and the small black square in the middle indicates where the servomotor was located and the servomotor was powered off during the measurement. The measurement was conducted on a planar (handwritten: surface) 10 cm above the servo.

nose setup. The plot (Fig 4: lower panel) shows that the influence introduced by adding the mount on the nose is negligibly small with the magnitude of lift forces being around 1 N compared to the total lift force of the UAV, up to 60 N (as it should balance a mass of 6 kg). (handwritten: carry (payload?) kg) In principle, the center of gravity (CG) can be fixed by adjusting the battery position and some changes in the moment of inertia can be easily handled by the flight controller. A flight test with this setup showed stable behavior of

135   the UAV, and the change in the moment of inertia is within the capabilities of the flight controller. Increased boom lengths theoretically do not cause significant aerodynamic forces as the rod is parallel to the airflow or at small angles of attack during the flight. (handwritten: – NO, but it does increase instability.) (handwritten: Find better word.)

Based on the result of the static experiment and the aerodynamic analysis, we slightly tweaked the initial set-up as shown in Fig 4, still mounting two magnetometers on a boom mounted on the noise-tip but now with both sensors further away from the

140   aircraft (Fig 5) to reduce the amount of noise on the sensors and provide a solution where filtering out magnetic noise from the UAV becomes easier (Chen et al., 2018; Mu et al., 2020). (handwritten: how? What about increased vibration?)

The second iteration of the setup comprises the installation of two compact magnetometers from QuSpin, abbreviated as QTFM. The QTFM is a compact, low power, and high-sensitivity scalar magnetometer, capable of sampling the geomagnetic field over 200 times per second (Table 2). The primary magnetometer (front magnetometer) is responsible for measuring the

145   signal of interest, whereas the secondary sensor placed closer to the nose-tip is used to monitor the in-flight noise from the platform. The distance d is used to indicate the distance between the primary and secondary magnetometer, whereas L is for the distance between the secondary magnetometer and the mounting point on the UAV (see Fig 5).
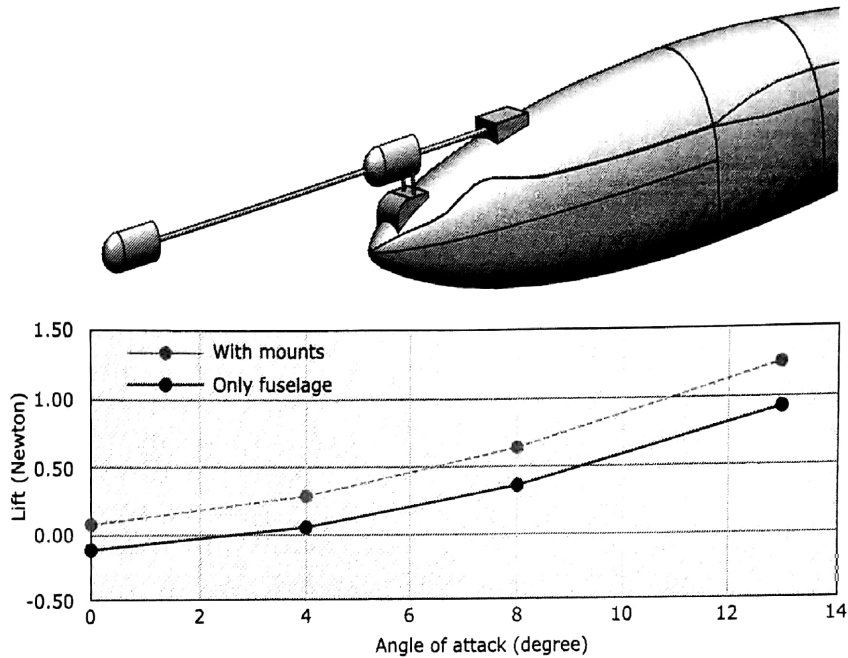
Geoscientific
Instrumentation
Methods and
Data Systems
Discussions
Open Access

Figure 4. The nose-mounting solution and its aerodynamics simulation.
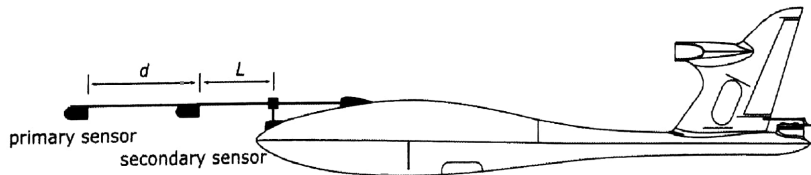

Figure 5. The final design of the front-boom-mounting setup and a side view of the hybrid VTOL fixed-wing in this study.

5 UAV in-flight magnetic signature - dynamic experiment

5.1 Method

150 Dynamic effects such as magnetic field generated by revolving solenoids or permanent magnets, eddy current in the airframe, or maybe even loose wires can produce either discontinuous or continuous noise. Discontinuous noise appears as isolated spikes or set of closely-spaced spikes on the aeromagnetic data, which is typically associated with the pilot's actions such as radio transmissions or switching direct current and to lightning strikes or cultural sources (e.g. train, power lines) (Reeves, 2005; Eppelbaum, 2011, 2015). Continuous noise comes from the motions of the aircraft, such as the oscillation of wings while

155 in flight through turbulent weather, which produces a high-frequency unwanted noise signal. The empirical fourth difference function is widely used for monitoring the level of such in-flight noise in aeromagnetic data to ensure that the noise is within an acceptable level (Reeves, 2005). Complying with the widely-accepted industry standard, the fourth difference should lie

Geoscientific
Instrumentation
Methods and
Data Systems
Discussions

Open Access

Table 2. Specifications of QuSpin Total Field Magnetometers (QTFM)

Parameters	
Field sensitivity	smaller than 1pT in 0.1 Hz - 100 Hz band
Dynamic range	1,000 nT to 100,000 nT
Max data rate	400 samples/s ← True ?
Dead zone	single equatorial plane, ±7 deg
Atomic species	Rubidium
Power	5V to 19V, 2 W total (sensor+electronics), 3W during startup
Heading error	below 3 nT (uncompensated)

between ±0.05 nT (or 0.1 nT peak to peak) (Coyle et al., 2014; Cunningham, 2016). The fourth difference for an airborne magnetic survey can be calculated as

160

$$\text{4th difference} = -\frac{T_{-2} - 4T_{-1} + 6T_0 - 4T_{+1} + T_{+2}}{16},\tag{1}$$

where T_{-2}, T_{-1}, T_{+1}, and T_{+2} are five consecutive readings centered on the current reading T_0.

To understand the real dynamic noise of the UAV in operation, we flew two dynamic experiments in Støvring, Denmark (Fig 6). The test site is covered with up to 12 km of unmetamorphosed sediments lodged over the crystalline basement, and the surface of the region consists mainly of unconsolidated Quaternary glacial and interglacial deposits (Håkansson and Surlyk,

165 1997). Normally, sediments are considered non-magnetic, which is the basis for many applications of aeromagnetic surveys (Reeves, 2005). As a result, the local magnetic field is insignificant, which renders the data collected during the dynamic experiment a direct reflection of the dynamic noise from the platform.

5.2 The first dynamic experiment - multi-rotor mode

The first dynamic experiment was flown on 2020.01.13. The front-mounting boom (Fig 5) was configured as d = 20 cm and

170 L = 20 cm. The sampling rate of the QTFMs was set to 200 Hz. The UAV was switched on and all required components such as the magnetometers and the power supply for the system, etc., were in position. At first, the UAV was placed on the ground and the pilot was conducting the last-minute check. This led to a moment at which the magnetometers could observe dynamic interference from the UAV irrelevant to motions. In this immediate pre-take-off phase (hereafter called "standby phase") and with only a few UAV components being active, the power consumption of the UAV should be low, and the current in the

175 wires connecting the battery with the flight controller should be low as well. As a result, the observed magnetic interference in the standby phase should arise from the current-carrying wires in the fuselage, permanent magnets of the actuators, and radio transmission along with may dynamic and/static cultural noise in the vicinity. Figure 7 shows residual magnetic intensity (RMI) with the International Geomagnetic Reference Field (IGRF) being removed from the raw magnetic measurements collected in the standby phase. As seen, the plots show continuous measurements of a superimposed magnetic field by the local geology (a
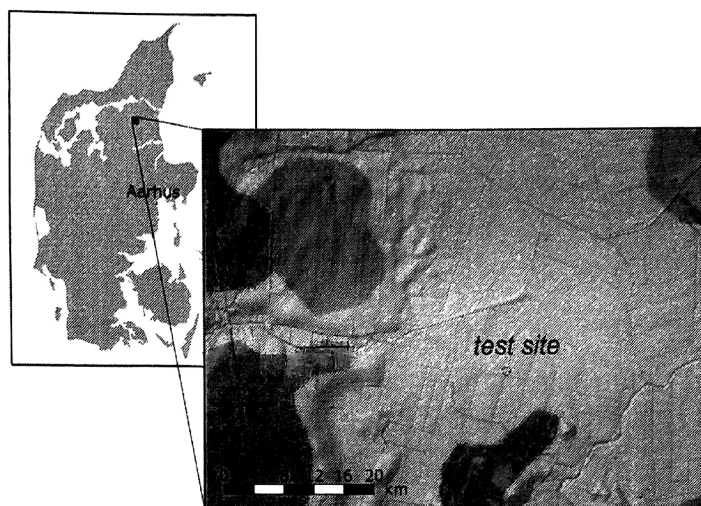
Legend

- Glaciofluvial sand and gravel
- Downwash sandy deposits
- Pre-Quaternary
- Sandy and gravelly till
- Freshwater deposits: peat, gyttja, clay silt and sand

Figure 6. Location and surface geology of the test site according to Surface Geology Map of Denmark 1:200000. The surface geology map of Denmark 1:20000 is credited to Schack Pedersen et.al., Surface Geology Map of Denmark, PDF, Version 2, compiled for the scale 1:200000, published in GEUS report 2011/19 (in Danish) by Geological Survey of Denmark and Greenland (GEUS), and the map of Denmark is credited to MAPSVG.COM.

180 constant offset), magnetic interference from the UAV, and cultural noise in the vicinity. The RMI in Fig 7 is oscillating around 2.8 nT with mean variations less than 0.5 nT, probably due to radio transmission and cultural noise. The average difference between the data from the primary and secondary magnetometer in this configuration is around 45 nT, which means that the longitudinal gradient between the primary and the secondary magnetometers is up to 225 nT/m (45 nT divided by 0.2 m), even when the UAV is on standby. The fourth difference of the measurements from the primary magnetometer is spiky and lies within

185 ±0.15 nT, significantly higher than the industry standard. Moreover, the discontinuous noise of the secondary magnetometer (Fig 7) is stronger, up to ±1 nT. The difference in the fourth difference indicates that the interference mainly originated from the UAV rather than the surroundings. Otherwise, the fourth difference of the two data sets should be comparable, because the secondary magnetometer is closer to the source of interference than the primary magnetometer. The distance between the two magnetometers attenuates the interference, leading to the smaller fourth difference of the data outputted by the primary

190 magnetometer.

Following the standby phase, the UAV took off and was flown only in the multi-rotor mode manually. Figure 8 and 9 show the in-flight residual magnetic intensity collected by both the primary and secondary magnetometer together with their
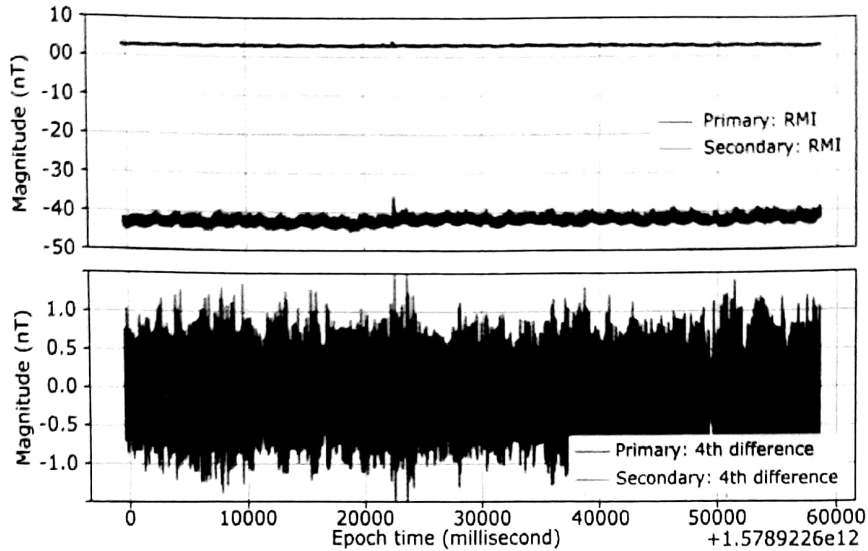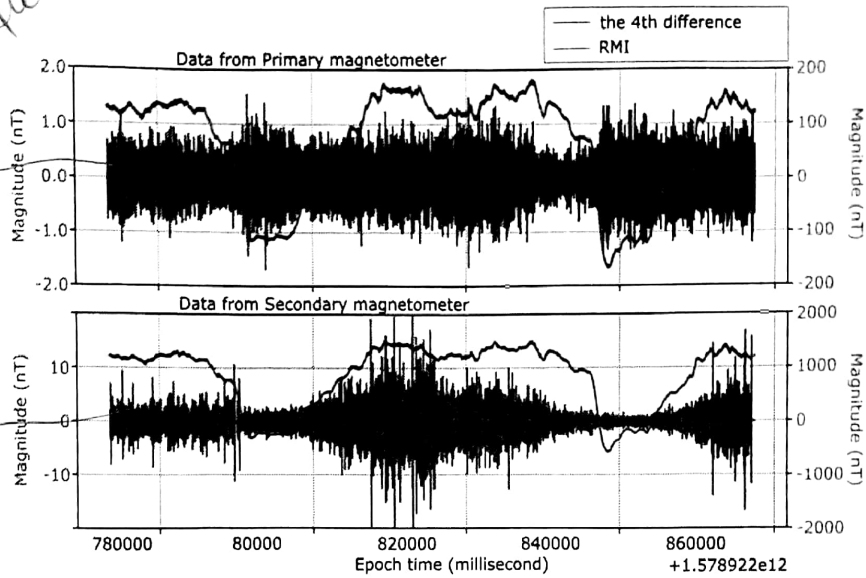
Figure 7. Data excerpt of the RMI and the fourth difference by the primary and secondary magnetometer while the UAV was on standby on 2020.01.13 with d = 20 cm and L =20 cm. The IGRF (50560 nT) has been removed.

corresponding fourth difference and its flight track. The two plots of the residual magnetic intensity in the figure show an identical pattern. The only difference lies in the magnitude with the RMI from the primary magnetometer being 10 times smaller than that from the secondary magnetometer. This indicates that the observed signals from the two magnetic sensors were dominated by the noise from the platform itself. An obvious reason for this behavior could be the multi-rotor flight mode with high output current flowing in the wires connecting the flight controller to the battery and the leakage of the magnetic field from the BLDC motors. In the standby phase, we observe a magnetic field of only around 2.8 nT (taken from the primary magnetometer). However, the in-flight fourth difference of the primary data in Fig 8 is spiky with magnitudes up to ±1 nT, also higher than the industry standard. Apparently, this increase is directly associated with the platform. Nevertheless, in principle, such strong noise can still be reduced distancing the magnetic sensors even farther away from sources of magnetic interference.

11

Geoscientific
Instrumentation
Methods and
Data Systems

Discussions

[handwritten annotation: Does the 4th difference of the two RMI's correlate? Why not?]

Figure 8. Data excerpt of the RMI by the primary and secondary magnetometer while the UAV was flown manually in the multi-rotor mode on 2020.01.13 with d = 20 cm and L = 20 cm. The IGRF (50560 nT) has been removed.

[handwritten annotation: constant removed?]
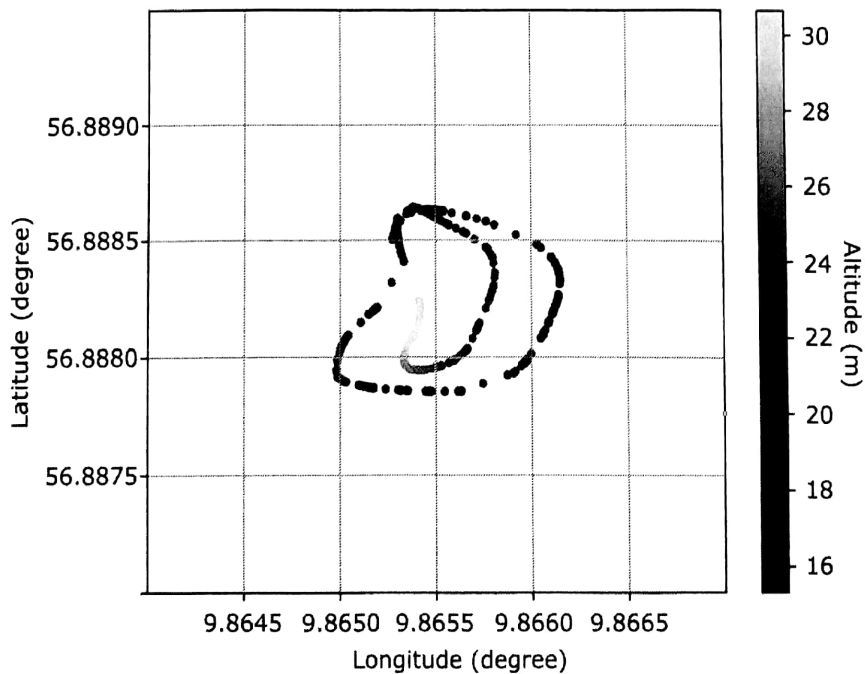
Figure 9. The production flight of the data excerpt. The altitude indicates the in-flight height above mean sea level.

(handwritten margin notes: "will first make a ratio of ... difference ... ratio of Ampere's law." and "$B_1 = \frac{R_0}{R_0 + (L_1 - L_0)} \cdot B_0$")

(handwritten left margin: "DON'T START A SENTENCE WITH BECAUSE")

## 5.3 The second dynamic experiment - fixed-wing mode

Because of the demonstrated strong interference from the UAV in the previous experiment, we increased the distance between the secondary magnetometer and the mounting point to $d = 20$ cm and $L = 30$ cm to improve the signal-to-noise ratio. In

205 addition, we planned an experiment in the fixed-wing mode to reduce the dynamic noise observed in the first experiment. Given that the changes may lead to in-flight instability, we required the pilot to fly the UAV manually in the fixed-wing mode. The sampling rate of the QTFMs was 200 Hz as well. Similarly, we show residual magnetic intensity in the standby phase (Fig 10) and then during the fixed-wing flight (Fig 11, 12, 13 and 14). *(handwritten: STOP USING TRANSITION WORDS.)*

In comparison with the data gathered in the previous experiment, there is a noticeable increase in magnitude of the RMI

210 in Fig 10, probably owing *(handwritten: due)* to the fact that the amount of direct current flowing in the wires, the orientation of the wires, and even the actual distance between the magnetometers and the wires were changed while we were preparing the system in the field. Besides, an extra metal GPS antenna was deployed inside the fuselage to timestamp magnetic recordings during the first experiment, which was solely used at the beginning to synchronize the sensors, after which it was removed to reduce the magnetic interference. Nevertheless, the difference between the actual measurements was still surprisingly big, up to 106 nT,

215 leading a longitudinal gradient of 530 nT/m. The second experiment was conducted at the same test site as the first one, so the local geomagnetic field should remain roughly constant. Consequently, this strong gradient must be somehow introduced by the platform. Interestingly, the fourth difference from the measurements from the secondary magnetometer is relatively bigger than that of the data from the primary magnetometer, but comparable, both within an envelope of ± 0.2 nT. Therefore, since the fourth difference of the primary and secondary magnetometer is comparable in magnitude, it is difficult to say whether the

220 noise originates mainly from the platform itself or cultural noise in the vicinity. However, it is clear that with the longer boom, the signal-to-noise ratio irrelevant *(handwritten: in relation to)* to aircraft maneuvers is improved significantly especially for the secondary magnetometer.

Furthermore, Figure 11 and 12 present RMI from both magnetometers and current load from the battery monitored by the onboard system in the flight from the take-off to the fixed-wing cruise accompanied by their corresponding fourth difference. Take Fig 11 for example - the first part of the RMI (outlined with dark grey box) was collected in the take-off phase (in the

225 multi-rotor mode), whereas the rest was measured in the fixed-wing cruise phase. And the gaps in the plot of the RMI were due to in-flight maneuvers of the UAV somehow rendering the QTFMs falling into dead zones at those moments.

The two plots of the RMI in Fig 11 and 12 are two visually identical, akin to the previous experiment. But the two plots visually look smoother than the data collected in the multi-rotor mode. Besides, a clear correlation is observed between the RMI and the output current from the battery, especially during the take-off phase, but later after transitioning to fixed-wing mode,

230 there is a clear decrease in the current and the magnetic field decreases accordingly. The magnitude of the two plots in Fig 14 are quite comparable before 1.583412e12 + 110000 millisecond *(handwritten: ms)* (epoch time since 1970.01.01), but after that moment, the magnitude increases significantly, five times bigger, which means that the secondary magnetometer is still highly susceptible to the inference from the UAV. Besides, the plots of the RMI in Fig 14 show a visually clear correlation with the pitch. The fourth difference of the in-flight measurements of the primary magnetometer during the fixed-wing cruise is around ± 0.2 nT

*(handwritten bottom: "(call it GPS time -" "(also do the math).")*
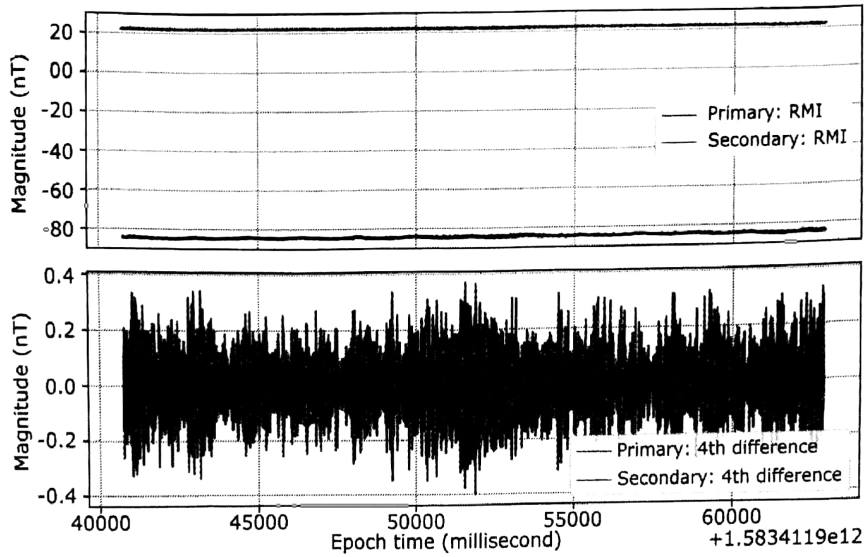
Figure 10. Data excerpt of the RMI and the fourth difference by the primary and secondary magnetometer while the UAV was on standby on 2020.03.05 with d = 20 cm and L = 30 cm. The IGRF (50563 nT) has been removed.
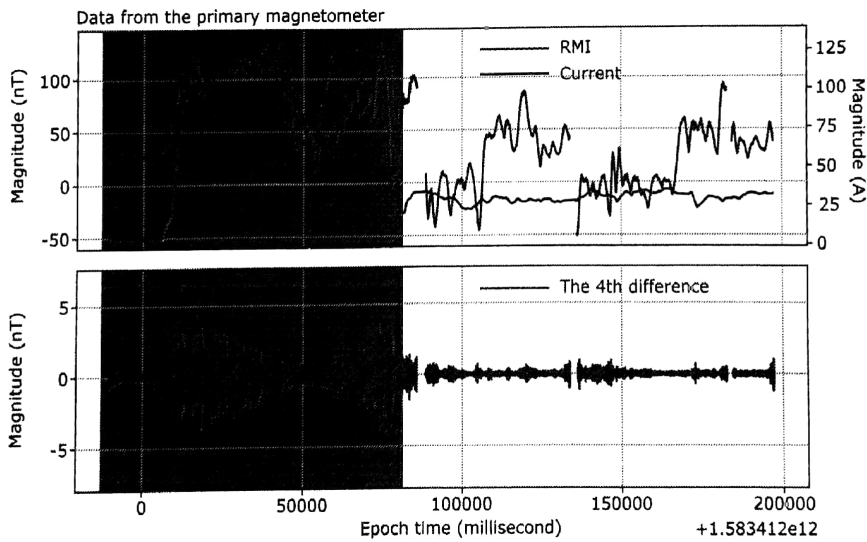

Figure 11. Data excerpt of the RMI by the primary magnetometer while the UAV was manually flown in the fixed-wing mode on 2020.03.05 with d = 20 cm and L = 30 cm. The IGRF (50563 nT) has been removed.

235   (Fig 14), slightly higher than the data collected before the take-off. It is evident that the fixed-wing mode gives less noisy data as expected.

14

Geoscientific
Instrumentation
Methods and
Data Systems
Discussions
Open Access
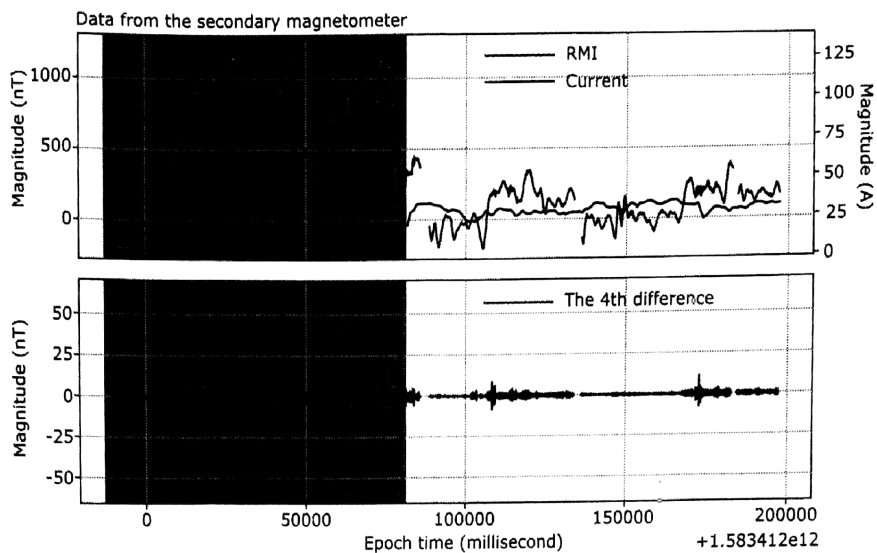
Figure 12. Data excerpt of the RMI by the secondary magnetometer while the UAV was manually flown in the fixed-wing mode on 2020.03.05 with d = 20 cm and L = 30 cm. The IGRF (50563 nT) has been removed
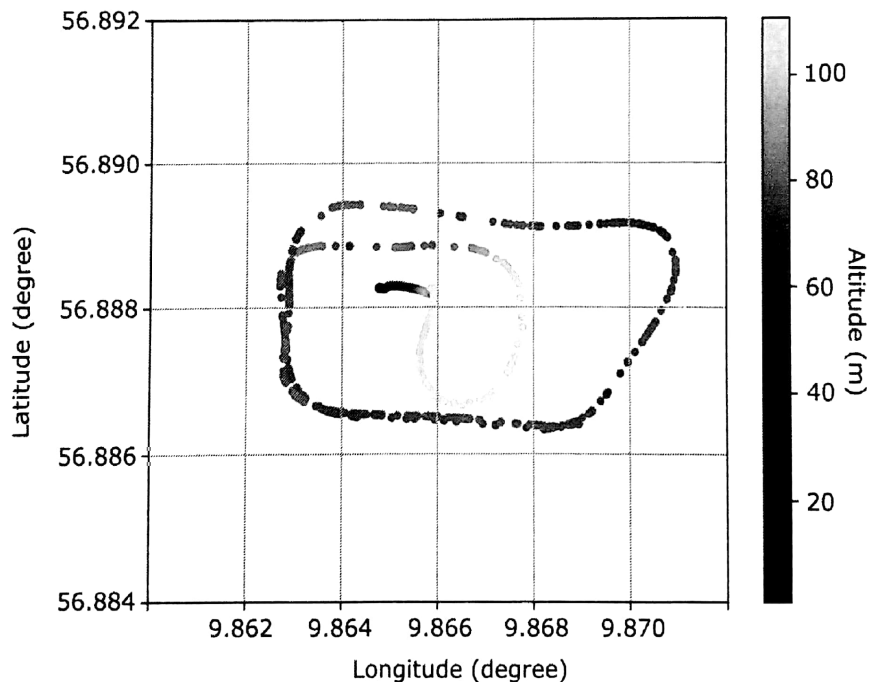
Figure 13. The production flight of the data excerpt. The altitude indicates the in-flight height above mean sea level.
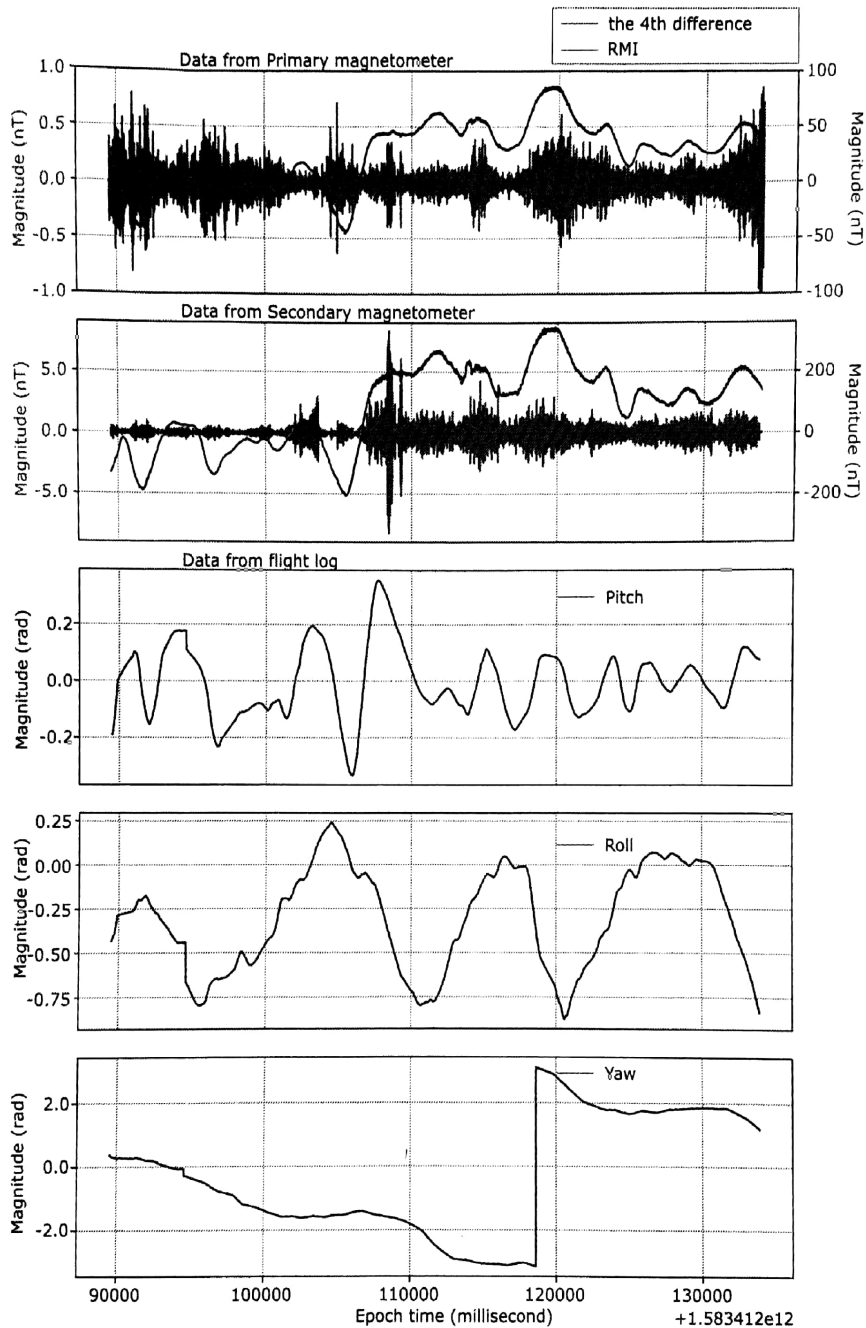
Figure 14. The RMI of the second segment from left to right in Fig 11 and 12 and the corresponding attitude from flight log.

6 Discussion

Based on the static and dynamic experiments, it is obvious that the magnetic interference from the platform is rather complicated, especially when the platform is in flight. From the static magnetic interference mapping, we have acquired insights into
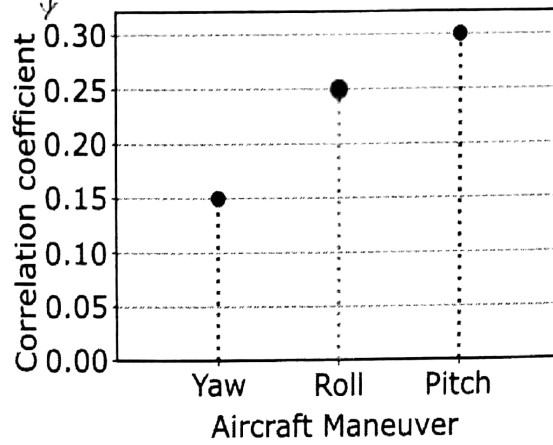
16

240   some potential regions on the platform. However, solely measuring static magnetic signature is not sufficient to provide decisive information for the development of an airborne magnetometry system. Therefore, trying to address the complex interplay between the onboard electronic components is more practical and important, especially when the platform is properly powered and in operation. For example, the static magnetic signature indicates that the interference at the primary and the secondary magnetometer is minimal and the longitudinal difference is less than 5 nT. Hence, during the static magnetic interference mea-

245   surement, the major interference is due to the permanent magnets of the electric actuators and electric motors. However, while the platform is powered and flying in operation, the magnetic interference increases significantly. The reason for the increase can be magnetic leakage of the electric actuators and electric motors, the magnetic field generated by dynamically-varying current flowing from the battery to flight controller, and the magnetic interference due to eddy current in the airframe. Interestingly, in comparison with the first dynamic experiment, the magnetic interference has also changed considerably in the second

250   dynamic experiment in the standby phase. In principle, the longer boom provides increased distance to sources of interference leading to stronger attenuation of interference from the platform, but on the contrary, the longitudinal gradient between the primary and the secondary magnetometers increased by ten times than that in the first dynamic experiment. The first variable between the two dynamic tests is power consumption because the platform consumes way more power in the multi-rotor mode than in the fixed-wing mode, which leads to strong current in the wires. The second variable is the layout of the components

255   inside the fuselage on-site such as the orientation of the wires connecting the battery with the flight controller. Besides, we also find out that the wires are quite soft so that the wires can actually move freely inside the fuselage due to inertia once the aircraft's attitude or speed changes and also it is clear that the transversal dimension of the fuselage on the platform is way smaller than the longitudinal dimension (see Fig 3), so once the wires start moving, there is more space for the wires to move along the longitudinal axis of the UAV than that along other axes. It can explain why the RMI in Fig 14 shows stronger corre-

260   lation with the pitch other than the superimposition effects of all the maneuvers, even though the roll changed more violently than the pitch (Fig 14 and 15).

      Regarding the issues, we have discovered, we first agreed to further increase the distance between the magnetometers and the platform without compromising the flight stability, because the noise envelop at the moment is too high to meet the industry standard for mineral exploration. Second, the wires connecting the battery and the flight controller should be properly placed

265   and shielded to further reduce the interference. Therefore, the next step is to consider how and where the components inside the fuselage should be placed.

7   Conclusions

We presented a static experiment, and based on the assessment of the results of the static experiment, we proposed a front-boom mounting system, of which stability is supported by our aerodynamic simulations. Later we conducted two dynamic

270   experiments to understand in-flight noise in operation. The results are insightful because surprisingly the strongest interference comes from the wires connecting the Li-Po battery to the flight controller. As a consequence, we propose to increase the distance between the magnetic sensors and the UAV again. Besides, we will try to shield the magnetic interference coming for

Geoscientific
Instrumentation
Methods and
Data Systems

Discussions

that is not significant correlation...

Figure 15. Correlation coefficient of the RMI and aircraft maneuvers.

the wires and also try to put the cable in the back of the fuselage to further keep the interference away from the magnetic field observation system.